Applied Microbiology and Biotechnology (2024) 108:446
https://doi.org/10.1007/s00253-024-13277-1

BIOTECHNOLOGICAL PRODUCTS AND PROCESS ENGINEERING

Kinetic characterization of two neuraminic acid synthases and evaluation of their application potential

Mehmet Mervan Çakar[1] · **Nevena Milčić**[1] · **Theofania Andreadaki**[2] · **Simon Charnock**[2] · **Wolf-Dieter Fessner**[3] · **Zvjezdana Findrik Blažević**[1]

Received: 20 May 2024 / Revised: 2 August 2024 / Accepted: 6 August 2024

Abstract

Neuraminic acid synthases are an important yet underexplored group of enzymes. Thus, in this research, we performed a detailed kinetic and stability analysis and a comparison of previously known neuraminic acid synthase from *Neisseria meningitidis*, and a novel enzyme, PNH_5, obtained from a metagenomic library. A systematic analysis revealed a high level of similarity of PNH_5 to other known neuraminic acid synthases, except for its pH optimum, which was found to be at 5.5 for the novel enzyme. This is the first reported enzyme from this family that prefers an acidic pH value. The effect of different metal cofactors on enzyme activity, i.e. Co^{2+}, Mn^{2+} and Mg^{2+}, was studied systematically. The kinetics of neuraminic acid synthesis was completely elucidated, and an appropriate kinetic model was proposed. Enzyme stability study revealed that the purified enzyme exhibits changes in its structure during time as observed by differential light scattering, which cause a drop in its activity and protein concentration. The operational enzyme stability for the neuraminic acid synthase from *N. meningitidis* is excellent, where no activity drop was observed during the batch reactor experiments. In the case of PNH_5, some activity drop was observed at higher concentration of substrates. The obtained results present a solid platform for the future application of these enzymes in the synthesis of sialic acids.

Key points

- *A novel neuraminic acid synthase was characterized.*
- *The effect of cofactors on NeuS activity was elucidated.*
- *Kinetic and stability characterization of two neuraminic acid synthases was performed.*

Keywords Biocatalysis · Neuraminic acid synthase · Sialic acids · Enzyme kinetics · Enzyme stability

Introduction

Sialic acid synthases are an underexplored family of enzymes, especially from the perspective of their application potential. Still, their role and function in physiological processes are more or less well defined. Prominent members of this family are *N*-acetylneuraminic acid synthases (NeuSs) that catalyse the formation of *N*-acetylneuraminic acid (Neu5Ac) by an aldol-like condensation of *N*-acetylmannosamine (ManNAc) and phosphoenolpyruvate (PEP) (Scheme S1). NeuS enzymes represent attractive targets for protein engineering, in order to alter their properties and provide easy irreversible enzymatic routes towards a wide range of sialic acid analogues (Knorst 1999; Suryanti et al. 2003; Schnellbächer 2017). The latter are very interesting compounds with a potential to serve as novel chemotherapeutic agents against bacterial and viral infections (Koketsu et al. 1997; Gunawan et al. 2005; Mertsch et al. 2020b; Mertsch et al. 2020b; Heida et al. 2021), as well as cancer and immunological disorders (Suryanti et al. 2003; Keil et al. 2022). Sialic acids, a structurally diverse group of more than 50 distinct negatively charged α-keto acids, are

✉ Zvjezdana Findrik Blažević
zfindrik@fkit.unizg.hr; zfindrik@fkit.hr

[1] University of Zagreb, Faculty of Chemical Engineering and Technology, Trg Marka Marulića 19, 10000 Zagreb, Croatia

[2] Prozomix Limited, Station Court, Haltwhistle, Northumberland NE49 9HN, UK

[3] Institute of Organic Chemistry and Biochemistry, Technical University of Darmstadt, Peter-Grünberg-Strasse 4, 64287 Darmstadt, Germany

widespread in viruses, mammalian cells, and microorganisms controlling a variety of biological functions, such as development, recognition, cell signalling, cell–cell interactions, and adhesion (Varki 1993, 1997; Traving and Schauer 1998; He et al. 2011; Yi et al. 2013; Fessner et al. 2014; Schnaar et al. 2014; Colley et al. 2014). They are terminal components of glycoproteins and glycolipids (Mertsch et al. 2020a). During the embryonic development of vertebrates, neural cell adhesion molecules are sialylated, which allows neural tissue to develop properly (Cunningham et al. 1983). Additionally, in certain cancers, sialylation of the cell surface is correlated with tumorigenesis and metastasis suggesting that sialic acids have a significant influence on human morbidity (Fukuda 1996; Gorelik et al. 2001; Yi et al. 2013). Among the sialic acids in nature, Neu5Ac is the most common and best studied sialic acid (Yi et al. 2013; Mertsch et al. 2020a), which due to their biological profiles are of potential importance for commercial application, i.e. as pharmaceutical precursors for antiviral drugs (e.g. Zanamivir (Zhang et al. 2010; Mertsch et al. 2020b)), food supplements and drug delivery systems nanocarrier stabilizers (Gurung et al. 2013). Since relatively simple structural modifications of sialic acids may significantly change their biological activities (von ltzstein and Thomson 1997), it can be expected that the synthesis of novel derivatives will have a strong potential of bringing innovative medicines to the market (Kiefel and Von Itzstein 2002). Although there are chemical methods for the preparation of Neu5Ac analogues (Warwel and Fessner 2000), sustainable and effective enzymatic methods of preparation will be of great interest for the synthesis and production of pharmaceutically active compounds based on Neu5Ac. Some research was already done on this topic (Mahmoudian et al. 1997; Knorst 1999; Schnellbächer 2017).

Current sources of microbial neuraminic acid synthases are rather scarce. They were first discovered in pathogenic microorganisms, and the first enzyme was isolated and purified from *Neisseria meningitidis* (Blacklow and Warren 1962). Later, the enzyme was isolated and purified to homogeneity from *Escherichia coli* K1 (Vann et al. 1997) and then found in *Campylobacter jejuni* (Linton et al. 2000) and *Streptococcus agalactiae* (Suryanti et al. 2003). Also, enzymes from the fish pathogens *Aliivibrio salmonicida* (Gurung et al. 2013) and *Moritella viscosa* (Berg et al. 2015) were discovered, of which the latter is the first cold-adapted neuraminic acid synthase. The first enzyme from a non-pathogenic source was discovered in *Idiomarina loihiensis*, a microorganism found in a submarine volcano in Hawaii (García García et al. 2015). Studies up to 2002 were mostly limited to genetic context and detection of activity (Hwang et al. 2002). In most studies, only a basic kinetic analysis of enzyme activity was performed, meaning that the Michaelis constants for PEP and ManNAc were estimated, as well as the maximum reaction rates, and/or catalytic constants (Table S1). It should be also noted here that different assays were used to determine enzyme activity. As these enzymes are cofactor dependent, different divalent metal ions were tested, and for most of them, divalent manganese, magnesium, and cobalt were found to be the most appropriate choices. The first structural study by CD spectroscopy and MALDI-TOF was performed for *Ec*NeuS, along with chemical cross-linking studies (Hwang et al. 2002). The authors found that the C-terminal region of the protein has a significant role in catalytic activity and conformational integrity. Sundaram et al. (2004) performed the first stereochemical analysis with *Cj*NeuS. They also concluded that the purified enzyme was unstable and performed their research with a partially purified enzyme. Suryanti et al. (2003) investigated *Sa*NeuS and suggested that arginine residues present in the active site are involved in substrate recognition, Arg 305 being the only totally conserved. The crystal structure of neuraminic acid synthase was elucidated for the *N. meningitidis* enzyme (Gunawan et al. 2005), and the mechanism of the action was clarified as well (Gunawan et al. 2005; Liu et al. 2009). Among the neuraminic acid synthases reported so far, most of them come from mesophilic origin and one is from a psychrophilic organism (*M. viscosa*).

We investigated the natural reaction catalysed by *Nm*NeuS and a novel enzyme from the Prozomix Ltd panel named PNH_5, identified as a putative NeuS homolog through sequence analysis using the bioinformatics platform ProzOMIGO and explored the kinetics of the synthesis of Neu5Ac starting from ManNAc and PEP (Scheme S1) as a model system. This reaction represents a good potential for the synthesis of sialic acid analogues. Thus, this research can be viewed to establish a platform that reveals possible bottlenecks in the reaction system and offers potential solutions. Therefore, we were focused on understanding the way this enzyme performs in a synthesis reactor, paying attention to the process, i.e. the reaction kinetics and operational stability of the enzyme, as well as the stability of the enzyme in general. Given the novelty of PNH_5, we conducted bioinformatic analyses to elucidate its structural characteristics via homology modelling and establish its similarity to known NeuS enzymes. With the application of protein engineering on NeuS, native enzymes could be modified to accommodate various non-native substrates and provide novel compounds with pharmaceutical potential. Initial research into that direction has already been conducted (Joseph et al. 2013).

Materials and methods

Chemicals and plasmids

ManNAc was purchased from Glentham Life Sciences, UK. Neu5Ac, $MgCl_2$, $CoCl_2$, $MnCl_2$, imidazole, *o*-benzylhydroxylamine hydrochloride ($BnONH_2$·HCl), and pyridine were obtained from Acros Organics, Belgium. The *neuB* gene (GenBank: EFM03356.1) containing pET19b for *Nm*NeuS and *pnh*5 gene (GenBank: PP887683) containing pET28a equivalent for PNH_5 expression vectors in BL21 (DE3) cells were provided from a TU Darmstadt collection (Schnellbächer 2017) and Prozomix Ltd, UK, respectively. Trifluoroacetic acid and Tris buffer were from Fisher Bioreagents, USA. Acetonitrile was from VWR, USA. Synergi™ Fusion-RP (80 Å, 4 µm, 4.6 × 250 mm) HPLC column was from Phenomenex, USA. The methanol gradient grade was from J.T. Baker, USA.

Quantification of compounds by HPLC

The samples from the reaction mixture were analysed by HPLC equipped with a PDA detector at 215 nm (Shimadzu, Japan), and the analysis was performed at 50 °C. A gradient method was applied for the analysis with two mobile phases, i.e. mobile phase A: 0.1% (*v*/*v*) trifluoroacetic acid in ultra-pure water and mobile phase B: mixture of acetonitrile and water in a volume ratio 80:20 with the addition of 0.1% (*v*/*v*) trifluoroacetic acid. The gradient was programmed as follows: 10–34% B over 8 min, 34–37% B over 3 min, 37% B for 5 min, 37–50% B over 4 min, 50–100% B over 3 min, 100% B for 2 min, 100–10% B over 4 min, and 10% B for 3 min. The flow rate was 0.8 mL min^{-1}.

ManNAc, PEP, and Neu5Ac were derivatised before the analysis with $BnONH_2$·HCl (Garrabou et al. 2009; Česnik et al. 2019) by using the following modified procedure. A 10 µL of the reaction sample was mixed with 50 µL of the derivatisation solution (130 mM $BnONH_2$·HCl in pyridine, methanol and water mixture containing 66, 30, and 4% *v*/*v*, respectively) and incubated at 50 °C and 900 rpm for 60 min. Then, 500 µL MeOH was added, and samples were centrifuged for 5 min at 14 000 rpm. Then, they were filtered through 0.22 µm hydrophobic PTFE filters and analysed by using the method described above. The linearity of the calibration curve was up to 25 and 15 mM for ManNAc and Neu5Ac, respectively. The retention times of PEP, Neu5Ac, and ManNAc derivatives were 3.7, 11.4, and 12.4 min, respectively (Figs. S1–S3).

Purification of NmNeuS and PNH_5

E. coli BL21 (DE3) cells transformed with the *neuB* gene from *Neisseria meningitidis* (GenBank: EFM03356.1) (Bateman et al. 2021) containing recombinant plasmid (pET19b-Nme_*neuB*) were used for the overexpression of the protein of interest. A 5 µL of glycerol stock solution (OD_{600} = ~1.5) was inoculated into 10 mL of LB medium containing ampicillin (100 µg mL^{-1}) and incubated overnight at 37 °C and 180 rpm. A 4 mL from the starter culture was inoculated into 400 mL of Prozomix® modified TBp medium containing ampicillin (100 µg mL^{-1}) and incubated at 26 °C and 280 rpm for 22 h. After cultivation, the cells were harvested by centrifugation at 4000 rpm for 15 min. The cell pellets were resuspended in buffer A (20 mM sodium phosphate, 500 mM NaCl, 30 mM imidazole pH 7.5, 1.0 mg mL^{-1} lysozyme) and incubated on ice for 30 min. The resuspended cells were disrupted by sonication and insoluble cell debris and protein aggregates were removed by centrifugation (14,000 rpm, 40 min). The supernatant was filtered through a 0.45-µm filter and then applied to a 5 mL HisTrap™ HP column (GE Healthcare, USA), which was pre-equilibrated with buffer A. The column was washed with 25 mL of buffer A and the *Nm*NeuS was eluted with buffer A containing different imidazole concentrations. The collected fractions were analysed by SDS-PAGE (Laemmli 1970) to identify fractions containing pure protein. For PNH_5, cell-free extract (CFE) was mixed with buffer A, and the obtained lysate was clarified by centrifugation (14,000 rpm, 40 min). The supernatant was filtered through a 0.45-µm filter, and then the same procedure was used for the purification. The collected fractions were subjected to dilution up to a final volume of 50 mL with the reaction buffers (150 mM sodium phosphate pH 7.5 and sodium acetate pH 5.5 for *Nm*NeuS and PNH_5, respectively) containing 5 mM ethylenediaminetetraacetic acid (EDTA) for the removal of Ni^{2+} ions leaked from the HisTrap™ HP column during the purification process and other metals present. Enzyme solutions were concentrated with ultracentrifuge tubes (MM Amicon Ultracel-10 K). Subsequently, the concentrated enzyme samples were diluted and washed three times with reaction buffers aimed at the complete elimination of residual EDTA (Mónico et al. 2017). The concentrated enzyme solutions were again centrifuged for the removal of aggregates (14,000 rpm, 30 min). This process yielded 12 mL of *Nm*NeuS at a concentration of 1.21 mg/mL and 10 mL of PNH_5 at a concentration of 1.14 mg mL^{-1}, with specific activities of 9.52 U mg^{-1} and 3.76 U mg^{-1}, respectively.

Activity assay for the determination of neuraminic acid synthase activity

Neuraminic acid synthase (NeuS) activity was determined from the change in concentration of Neu5Ac formed in the metal-dependent condensation of ManNAc and PEP (Scheme S1). For the first activity screening, reactions were performed in sodium phosphate acid buffer (150 mM, pH 7.5). Subsequently, optimum reaction buffers were employed for each enzyme in the ensuing experimental procedures.

For the screening assays, the solution containing 5 mM PEP, 5 mM ManNAc, and 0.05 mM Co^{2+} was prepared in buffer in a total volume of 2 mL. The reactor was thermostated at 37 °C and shaked at 900 rpm. The reaction was started by the addition of 50 µL of 0.5 mg mL^{-1} stock solution of pure NeuS. Six samples were taken from the reaction mixture at specific time intervals and analysed as described above. Sampling was done for approximately 25 min, and from the linear slope of the curve, representing the change of Neu5Ac concentration in time, specific enzyme activity is calculated (Eq. 1) (*S.A.* specific enzyme activity, U mg^{-1}; *c* molar concentration, mM; V_r reactor volume, mL; V_{NeuS} enzyme volume, mL; γ_{NeuS} mass concentration, mg mL^{-1}):

$$S.A. = \frac{dc_{\text{Neu5Ac}}}{dt} \cdot \frac{V_r}{V_{\text{NeuS}}} \cdot \frac{1}{\gamma_{\text{NeuS}}} \left[\frac{\text{U}}{\text{mg}} \right] \quad (1)$$

One unit of *Nm*NeuS and PNH_5 activity was defined as the amount of enzyme needed to catalyse the formation of 1 µmol Neu5Ac per minute at 37 °C in 150 mM sodium phosphate buffer, pH 7.5 for *Nm*NeuS and 150 mM NaOAc buffer, and pH 5.5 for PNH_5, respectively.

Screening of putative PNHs from Prozomix

A metagenomic library of wild-type PNHs sourced from diverse locations within the United Kingdom (Marshall et al. 2021) was sought to evaluate their potential for the aldol-like condensation of ManNAc and PEP to yield Neu5Ac. Reaction mixtures containing initial concentrations of 5 mM PEP, 5 mM ManNAc, and 1 mM Co^{2+} were prepared in 150 mM sodium phosphate pH 7.5 in a total volume of 950 µL. Reactors were thermostated at 37 °C and shaked at 900 rpm. The reactions were initiated by the addition of 50 µL of 4 mg mL^{-1} of CFEs. Then, 10 µL of the initial and 24-h samples were taken from the reaction mixture and analysed as described previously to elucidate PNHs activity in the synthesis of Neu5Ac. Subsequently, the PNHs yielding Neu5Ac underwent further investigation aimed at determining their specific activity rates in the synthesis of Neu5Ac. This evaluation was conducted by employing the activity assay described in the aforementioned section with the concentration of PNH in the assay of 0.2 mg mL^{-1}.

Bioinformatic analysis and molecular modelling PNH_5

To gain a comprehensive insight into the structure–function relationship of PNH_5, bioinformatic analyses have been utilized. Amino acid sequences of NeuSs from UniProt (Bateman et al. 2021) were aligned with Clustal Omega (Sievers et al. 2011) (UniProt accession number for each NeuS amino acid sequence; *Neisseria meningitidis* serogroup B, Q7DDU0; *Aeromonas caviae*, Q9R9S2; *Aliivibrio salmonicida*, B6EHB9; *Campylobacter jejuni*, Q7BC41; *Edwardsiella ictaluri*, C5BCQ8; *Escherichia coli*, Q46675; *Moritella viscosa*, A0A090IGE4; *Pseudomonas aeruginosa*, Q8KH52; *Streptococcus* sp. HMSC069D09, A0A1F0CHD3). The graphical output of the multiple sequence alignment of NeuSs was prepared by using ESPRIPT 3.0 server (Robert and Gouet 2014) and *Nm*NeuS (PDB ID: 1XUZ) as secondary structure information. The homology model of PNH_5 was created using AlphaFold2 based on the published structures (PDB ID: 1VLI, 1VS1, 1WVO, 2WQP, 3G8R, 3UZJ, 4IPI, 4IPJ, 6NCS, 6PPW, 8H2C) (Berman et al. 2003; Eastman et al. 2017; Mirdita et al. 2017, 2019, 2022; Mitchell et al. 2019; Steinegger et al. 2019; van Kempen et al. 2023). The theoretical molecular weights of *Nm*NeuS and PNH_5 were calculated via Expasy compute pI/Mw tool (Gasteiger et al. 2005). The graphics were done by PyMOL (Molecular Graphics System, Version 2.0 Schrodinger, LLC).

The influence of buffer and pH on enzyme activity

The specific activities of *Nm*NeuS and PNH_5 were measured in 150 mM buffers; sodium acetate for pH 5–5.5, sodium phosphate for pH 6–8, Tris–HCl for pH 8.5, and glycine–NaOH for pH 9–10. The effect of pH on the activity of *Nm*NeuS was determined by incubating the reaction mixture (1 mL total volume) with selected buffers containing initial 5 mM concentrations of ManNAc and PEP, and 1 mM $MnCl_2$ for *Nm*NeuS and 10 mM concentrations of ManNAc and PEP, and 0.05 mM $CoCl_2$ for PNH_5, respectively. The reactors (1.5 mL Eppendorf tubes) were thermostated at 37 °C and shaked at 900 rpm. Sampling and analysis were done as described previously. The concentrations of *Nm*NeuS and PNH_5 in the assay were 0.0125 and 0.023 mg mL^{-1}, respectively.

Determination of enzyme kinetics

The enzyme kinetics were determined by using the initial reaction rate method. The influence of concentrations of all reaction compounds on the specific enzyme activity was evaluated, i.e. ManNAc, PEP, Neu5Ac, Co^{2+}, Mn^{2+}, and Mg^{2+}. The enzyme activity was calculated according to Eq. (1) based on the change in product concentration in time. During these measurements, the substrate conversion was always below 10%. The experimental conditions for each data series are presented in the legends below the corresponding figures. It needs to be noted here that the effect of concentrations of each compound was investigated independently, which means that all the other reaction conditions were kept constant. For example, when the influence of ManNAc concentration on enzyme activity was evaluated, all other concentrations were kept constant, i.e. PEP and

Co^{2+}. Experiments were performed at 37 °C on a shaker at 900 rpm. The volume of the reaction mixture was 1 mL, and the total sampling volume was always below 10%. The experiments were carried out in 1.5 mL Eppendorf tubes.

NmNeuS and PNH_5 storage stability

The evaluation of the enzyme storage stability was conducted through the integration of three methodologies, i.e. the assessment of enzyme activity using the activity assay described above, by following protein concentration using the Bradford method (Bradford 1976) and the quantification of protein size distribution through particle size distribution analysis (PSD). During storage, changes in protein structure occur and can lead to deactivation. These were followed by the dynamic light scattering (DLS) method. DLS is a highly sensitive technique capable of detecting particles ranging from sub-nanometre sizes up to several micrometres, depending on the specific instrument, which makes it suitable for detecting solvated protein molecules in homogeneous mixtures, as well as larger, insoluble aggregates. The characterization of particle distribution with varying hydrodynamic diameters (D_h) was achieved through the utilization of the number size distribution (NSD), the volume size distribution (VSD), and the intensity size distribution (ISD). NSD demonstrates the number of particles, serving as an indicator of relative protein concentration, and VSD demonstrates the volume that particles occupy. On the other hand, IDS represents the amount of light scattered by the particles in the sample, highlighting the presence of larger particles, which makes it particularly suitable for the early identification of aggregate formation. Increases in the size of protein molecules, exceeding those observed in enzyme crystal structures, are commonly ascribed to protein aggregation, a phenomenon detectable by monitoring PSD (Stetefeld et al. 2016; Milčić et al. 2022). Distributions were monitored by DLS on a Zetasizer Ultra (Malvern Panalytical, Malvern, United Kingdom). Pure *Nm*NeuS and PNH_5 enzyme stocks, stored at 4 °C in 150 mM of sodium phosphate buffer pH 7.5 (*Nm*NeuS and PNH_5) and 150 mM sodium acetate pH 5.5 (PNH_5), were analysed during approximately 50 days of storage. Bovine serum albumin (BSA), well-characterized protein in terms of size and distribution, was used as a standard, while each measurement of NeuS enzymes samples was preceded by control measurement with a buffer solution same as sample matrix. Each measurement was performed in triplicate with a temperature equilibration time of 120 s at 25 °C.

The influence of reaction conditions on enzymatic synthesis of Neu5Ac in batch reactor experiments

Two series of batch reactor experiments were conducted at different reaction conditions, i.e. substrates and enzyme concentration, one with *Nm*NeuS, and the other with PNH_5. During these experiments, the concentration of the reaction compounds was followed, as well as enzyme activity to evaluate the enzyme operational stability. Reactions of 15 mL containing ca. 10, 20, 50, and 100 mM equimolar concentrations of ManNAc and PEP and 0.05 mM of Co^{2+} were initiated in 15-mL centrifuge tubes by the addition of 0.021 and 0.053 mg mL^{-1} of *Nm*NeuS and PNH_5, respectively. Designated concentrations represent the amount of enzyme in the reaction mixture, i.e. reactor. They correspond to activities of 0.34 and 0.30 U mL^{-1} of *Nm*NeuS and PNH_5, respectively. Subsequently, the reaction mixtures were distributed in 1 mL aliquots among 15 conical 1.5-mL Eppendorf tubes for the facilitation of sample collection. They were placed on a shaker at 900 rpm and 37 °C. At predetermined time points, 10 μL of the reaction mixture was taken from each aliquot for the quantification of substrate and product concentrations. Then, 0.99 mL reaction mixture from each aliquot was used to isolate the enzyme and subsequently separate it from the other components of the reaction mixture via ultracentrifugation in Amicon™ Ultra-0.5 centrifugal unit (Merck, USA; 4 °C, 14 000 rpm, 5 min). After the first round of ultracentrifugation, the concentrated reaction sample underwent successive washes with reaction buffers (450 μL × 2 times) to eliminate all components except for the enzyme. Eventually, the obtained enzyme samples (100 μL) were employed to initiate the activity assays (*Nm*NeuS (10 mM PEP and ManNAc, 0.05 mM Co^{2+}, 990 μL total reaction volume); PNH_5 (20 mM PEP and ManNAc, 0.05 mM Co^{2+}, 1050 μL total reaction volume in 1.5 mL conical Eppendorf tubes)). In these experiments, the concentrations of compounds were followed by HPLC as described before and the activities of *Nm*NeuS, and PNH_5 were calculated according to Eq. (1).

Data handling and development of the mathematical model

The experimental data on the dependence of the specific enzyme activity on the concentration of reaction compounds was used to estimate the kinetic constants. For this purpose, program package SCIENTIST and non-linear regression analysis were used. Simplex and Least squares methods implemented in SCIENTIST were used for the estimation of the kinetic parameters. The same software was used for the simulation of data.

The reaction rate (r) of the aldol-like condensation of ManNAc and PEP catalysed by *Nm*NeuS was described by double substrate Michaelis–Menten kinetics (Eq. (2)), whereas for PNH_5, the inhibition by PEP was included in the model (Eq. (3)). In both equations, there is a factor f included (Eq. (4)). It defines the influence of cofactor Co^{2+} concentration on the reaction rate. Namely, it is known that enzyme activity is dependent upon the concentration of the cofactor. It is however put in a separate equation because the cofactor is not spent in the reactor, but it affects the reaction rate.

$$r_1 = \frac{V_m \cdot c_{\mathrm{ManNAc}} \cdot c_{\mathrm{PEP}} \cdot f \cdot \gamma_{Nm\mathrm{NeuS}}}{\left(K_m^{\mathrm{ManNAc}} + c_{\mathrm{ManNAc}}\right) \cdot \left(K_m^{\mathrm{PEP}} + c_{\mathrm{PEP}}\right)} \tag{2}$$

$$r_2 = \frac{V_m \cdot c_{\mathrm{ManNAc}} \cdot c_{\mathrm{PEP}} \cdot f \cdot \gamma_{\mathrm{PNH}_5}}{\left(K_m^{\mathrm{ManNAc}} + c_{\mathrm{ManNAc}}\right) \cdot \left(K_m^{\mathrm{PEP}} + c_{\mathrm{PEP}} + \frac{c_{\mathrm{PEP}}^2}{K_i^{\mathrm{PEP}}}\right)} \tag{3}$$

$$f = \frac{c_{\mathrm{CO}^{2+}}}{K_m^{\mathrm{CO}^{2+}} + c_{\mathrm{CO}^{2+}}} \tag{4}$$

Equations (5)–(7) represent the mass balance equation for ManNAc, PEP, and Neu5Ac in the batch reactor, which were used for the reaction simulation.

$$\frac{\mathrm{d}c_{\mathrm{ManNAc}}}{\mathrm{d}t} = -r \tag{5}$$

$$\frac{\mathrm{d}c_{\mathrm{PEP}}}{\mathrm{d}t} = -r \tag{6}$$

$$\frac{\mathrm{d}c_{\mathrm{Neu5Ac}}}{\mathrm{d}t} = r \tag{7}$$

If operational stability decay occurs, it was assumed that it will occur by the kinetic model of the first order according to Eq. (8):

$$\frac{\mathrm{d}V_m}{\mathrm{d}t} = -k_d \cdot V_m \tag{8}$$

Results

In this work, the biocatalytic synthesis of Neu5Ac was investigated via aldol-like addition of ManNAc and PEP. For this purpose, we investigated the previously known enzyme from *Neisseria meningitidis* and evaluated a panel of putative enzymes from Prozomix Ltd. After the initial screening and the selection of the best candidate, we performed a preliminary characterization of the new enzyme, followed by thorough kinetic analysis for both enzymes, revealing the differences and similarities between them. Further, we conducted a computational study to model the molecular structure of PNH_5 and its similarity to the currently known enzymes. We also focused on enzyme stability at both storage conditions and reactor conditions. A kinetic model of the synthesis reaction was developed and validated in the batch reactor.

Screening of putative homologues of neuraminic acid synthases

A panel of 13 putative homologues of NeuS from Prozomix Ltd (PNHs) was screened in the synthesis of Neu5Ac to find the best representative for further characterization according to the procedure described in the Experimental part. First, the enzymes were compared according to Neu5Ac production efficiencies (Fig. 1a). From these results, 5 hits, i.e. PNH_2, PNH_3, PNH_5, PNH_6, and PNH_{11}, were further characterized by comparing their specific activities (Fig. 1b) in the targeted reaction. The best activity was obtained with PNH_5, which was further characterized as a representative of the panel.

Bioinformatic analysis and molecular modelling of PNH_5

As PNH_5 showed the highest Neu5Ac production efficiency among the putative homologues, bioinformatic analyses were used to obtain a comprehensive insight into its structure–function relationship. The subsequent section aims to elucidate and interpret the implications of these analyses. The theoretical molecular weights of *Nm*NeuS and PNH_5 were calculated based on amino acid sequences as 38,347 and 38,377 Da, respectively. The accurate molecular weight of *Nm*NeuS was determined with ESI–MS as 38,649.8 Da (Hao et al. 2005). Therefore, the determined molar masses exhibit a close concordance with the computed values.

Fig. S4 illustrates a structural alignment depicting the sequence comparison of various NeuS homologs. Most residues associated with secondary structure elements exhibit either identical matches or preservation of similar physiochemical properties. Across different NeuB sequences, the amino acids crucial for ligand binding in *Nm*NeuS and PNH_5 (Mn^{2+}, PEP, and ManNAc) remain conserved. PNH_5 exhibits the highest sequence identity with NeuS from *Moritella viscosa* (62.43%).

Structure similarity of NmNeuS and PNH_5

Up to now, *Nm*NeuS is the only NeuS enzyme for which a crystal structure has been solved (Gunawan et al. 2005; Liu et al. 2009). The substrate binding situation can be gathered from a crystal structure of *Nm*NeuS that contains Mn^{2+}, PEP, and a reduced non-reactive analogue of ManNAc (rManNAc) (Gunawan et al. 2005). In addition, *Nm*NeuS has been crystallized with an analogue of the reaction intermediate (Liu et al. 2009). As seen in Fig. 2a, PNH_5 has been

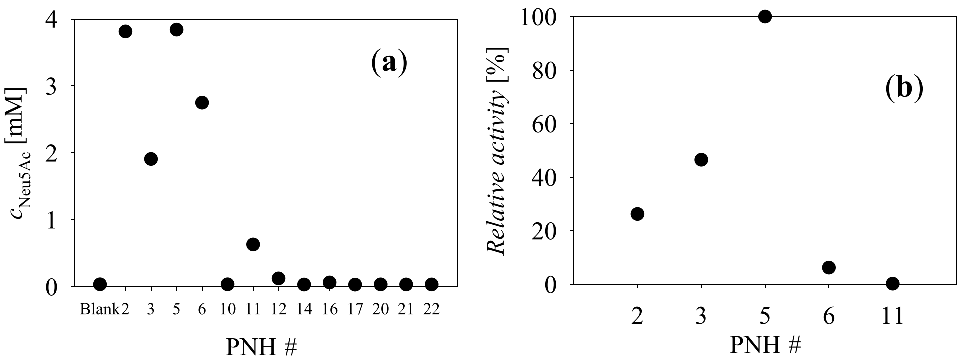

Fig. 1 **a** PNH panel screening in Neu5Ac synthesis via metal-dependent condensation of ManNAc and PEP catalysed by PNHs ($c_{ManNAc}=5$ mM, $c_{PEP}=5$ mM, $c_{Co}{}^{2+}=1$ mM, $\gamma_{PNH}=0.2$ mg mL^{-1}, 150 mM HEPES buffer pH 7.5, 24 h, $T=37$ °C). **b** Comparison of specific activities of the best selected PNHs from (**a**) ($c_{ManNAc}=10$ mM, $c_{PEP}=10$ mM, $c_{Co}{}^{2+}=0.05$ mM, $\gamma_{PNH}=0.2$ mg mL.$^{-1}$, 150 mM sodium phosphate buffer pH 7.5, $T=37$ °C)

identified as a domain-swapped homodimer. The monomers consist of a $(\beta/\alpha)_8$ catalytic barrel at the N-terminus coupled to an antifreeze protein-like (AFPL) domain at the C-terminus via an extended flexible linker region (Gunawan et al. 2005). The catalytic barrel of one monomer is capped by the AFPL domain on the other monomer during dimer assembly. As a result of the homology searches against type III antifreeze proteins, the AFPL domain had previously been identified and was suggested to function in polar sugar-substrate binding (Baardsnes and Davies 2001). It has since been demonstrated that the AFPL domain plays an essential role in the catalysis of *Nm*NeuS by contributing active site residues, which provide the catalytic orientation of the ManNAc within the active site (Joseph et al. 2013, 2014).

The corresponding model of PNH$_5$'s active site architecture with bound Mn^{2+}, PEP, and rManNAc is illustrated in Fig. 2b. The N-terminal domain of PNH$_5$ contributes most of the catalytic residues. Single residues Phe285 and conserved the Arg311 are contributed by the AFPL domain. Arg311 interacts directly with the N-acetyl carbonyl of rManNAc in *Nm*NeuS, while Phe285 forms part of the hydrophobic pocket. Phe285 is present in some members among the bacterial NeuS enzymes with AFPL domain, whereas Arg311 is completely conserved. Additionally, Arg311 is not present in AFPL domains of the mammalian Neu5Ac-9-phosphate synthase (Gunawan et al. 2005).

Furthermore, ManNAc interacts with Asp245, Gln53, and Tyr184 within the fully conserved catalytic residues besides Arg314. The C-6 hydroxyl of ManNAc interacts with Asn72, which contributes to the β2-α2 loop of the catalytic domain. While Asn72 is fully conserved in NeuS enzymes, it is not present in other sialic acid synthase enzymes. The phosphate group of PEP interacts via H-bonds with Ser130, Ser152, and Ser211 residues, which are fully conserved among the bacterial sialic acid synthases and mammalian Neu5Ac-9PSs. Additionally, the phosphate group of PEP also interacts with Asn182 which is not completely conserved among the sialic acid synthase family. The carboxylate group of PEP is interacting with the conserved Lys51 and Lys127 residues. While Thr108's reactive group is close to the PEP carboxylate, it is not within the hydrogen bonding range. Additionally, among the sialic acid synthase family, the residue is conserved as either Ser or Thr (Gunawan et al. 2005).

Imidazole chains of His213 and His234, which are fully conserved among both bacterial and mammalian sialic acid synthases, form interactions with Mn^{2+} at the active site owing to metal's octahedral geometry, indicating that the metal dependency is a key evolutionary characteristic of these enzymes (Gunawan et al. 2005).

The detailed analysis of PNH$_5$'s active site, encompassing interactions with Mn^{2+}, PEP, and ManNAc, underscores the significance of specific residues, such as Arg311 and Phe285, in catalytic orientation. Moreover, the conserved nature of key residues, including Asn72 and imidazole chains of His213 and His234, across bacterial and mammalian sialic acid synthases highlights the evolutionary importance of metal dependency in these enzymes. These findings not only enhance our understanding of PNH$_5$'s catalytic mechanism as a NeuS but also provide a foundation for further exploration into the broader functions and potential applications of NeuS enzymes in the context of sialic acid biosynthesis.

pH and temperature dependence of enzyme activity

The influence of pH on the activity of *Nm*NeuS and PNH$_5$ is presented in Fig. 3. While the *Nm*NeuS shows an optimum activity at pH 7.5 (Fig. 3a) just like reported by Hao et al. (2005), PNH$_5$ prefers acidic pH value and exhibits its

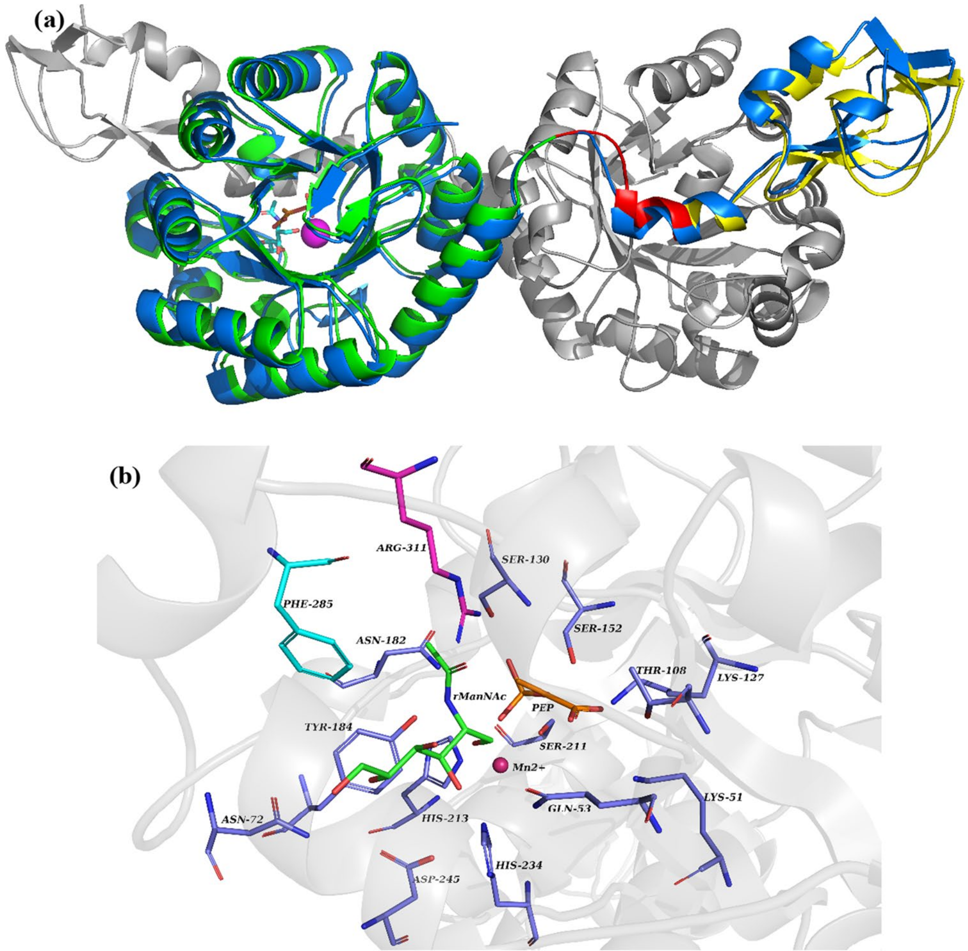

Fig. 2 **a** Homology model of PNH_5 dimer created with AlphaFold2 based on the published structures. PNH_5's Chain A is coloured grey, and Chain B is coloured by domain. The catalytic domain of PNH_5 chain B is shown in green (residues Met1-Gly271), the linker domain in red (residues Ser272-Val281), and the AFPL domain (residues Thr282-Glu346) in yellow. PNH_5 chain B monomer is superimposed with the structure of *Nm*NeuS monomer coloured blue. rManNAc is coloured cyan, PEP orange, and Mn^{2+} magenta. **b** PNH_5 active site. The N-terminal catalytic domain, linker region, and AFPL residues are coloured in blue, cyan, and magenta, respectively. rManNAc, PEP, and Mn^{+2} are coloured in green, orange, and pink, respectively

maximum activity at pH 5.5 (Fig. 3b). This is untypical for the NeuS homologs found so far and is reported for the first time for this enzyme family.

The effect of different buffers was evaluated for *Nm*NeuS, and the results are presented in Fig. S5 showing an optimum activity in HEPES buffer. The choice of pH 7.6 was made to investigate the impact of the buffer on the activity of *Nm*NeuS. Additionally, this pH value was selected to accommodate the inclusion of bicine buffer in the experimental buffer set. For practical reasons, sodium phosphate buffer pH 7.5 showing 91% of maximum activity was used in further

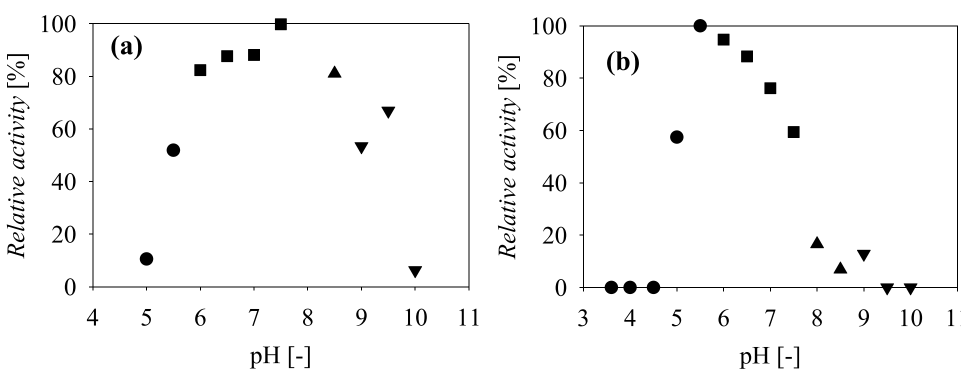

Fig. 3 Effect of pH on (**a**) *Nm*NeuS activity ($c_{ManNAc}=5$ mM, $c_{PEP}=5$ mM, $c_{Mn^{2+}}=1$ mM, $\gamma_{NeuS}=0.0125$ mg mL^{-1}, 150 mM buffer, 37 °C, 100% activity corresponds to 10.62 U mg^{-1}) and (**b**) PNH_5 activity ($c_{ManNAc}=10$ mM, $c_{PEP}=10$ mM, $c_{Co^{2+}}=0.05$ mM, $\gamma_{PNH5}=0.023$ mg mL^{-1}, 37 °C, 150 mM buffer, 100% activity corresponds to 5.02 U mg^{-1}). Legend: black circle, sodium acetate buffer; black square, sodium phosphate buffer; black triangle, Tris–HCl buffer; black triangle down, glycine–NaOH

characterization in the case of *Nm*NeuS, whereas sodium acetate buffer pH 5.5 was selected for PNH_5.

The influence of temperature on the activity of both enzymes is presented in Fig. 4. Both enzymes show an optimum activity at 50 °C. Considering the temperature profiles, 37 °C was chosen for subsequent experiments as the enzyme activity at this temperature is satisfactory, while stability is presumably higher than at the temperature optimum.

The influence of cofactor on the activity of NmNeuS and PNH_5

The results presented in Fig. 5. indicate that the influence of different concentrations of all three cofactors can be described by Michaelis–Menten kinetics for both *Nm*NeuS and PNH_5, respectively. Additionally, both enzymes exhibit the maximum activity in the presence of Co^{2+} ions as cofactor (Fig. 5c and 5f), which was highlighted in the work of Hao et al. (2005) for *Nm*NeuS. The experimental data (Fig. 5) were used to estimate the values of the kinetic parameters presented in Table 1. It can be concluded from the kinetic parameters that Mg^{2+}, even though it was often used with *Nm*NeuS (Blacklow and Warren 1962; Hao et al. 2005), is not a good choice because it suffers from the highest value of the apparent Michaelis constant. When it comes to PNH_5, Mg^{2+} is by far the worst cofactor, considering that the estimated maximum reaction rate is only 0.11 U mg^{-1}. Both enzymes exhibit high affinity towards

Fig. 4 Effect of temperature on (**a**) *Nm*NeuS activity ($c_{ManNAc}=5$ mM, $c_{PEP}=5$ mM, $c_{Mn^{2+}}=1$ mM, $\gamma_{NeuS}=0.0125$ mg mL^{-1}, 150 mM sodium phosphate buffer, pH 7.5) and (**b**) PNH_5 activity ($c_{ManNAc}=10$ mM, $c_{PEP}=10$ mM, $c_{Co^{2+}}=0.05$ mM, $\gamma_{PNH5}=0.023$ mg $mL.^{-1}$, 150 mM sodium acetate buffer pH 5.5)

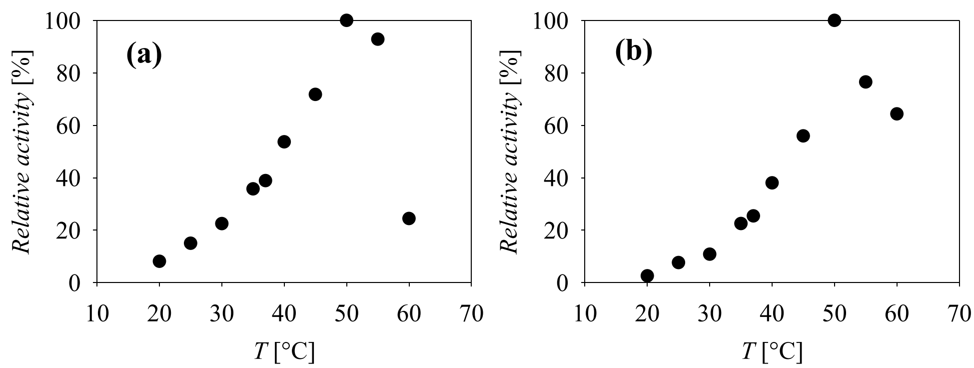

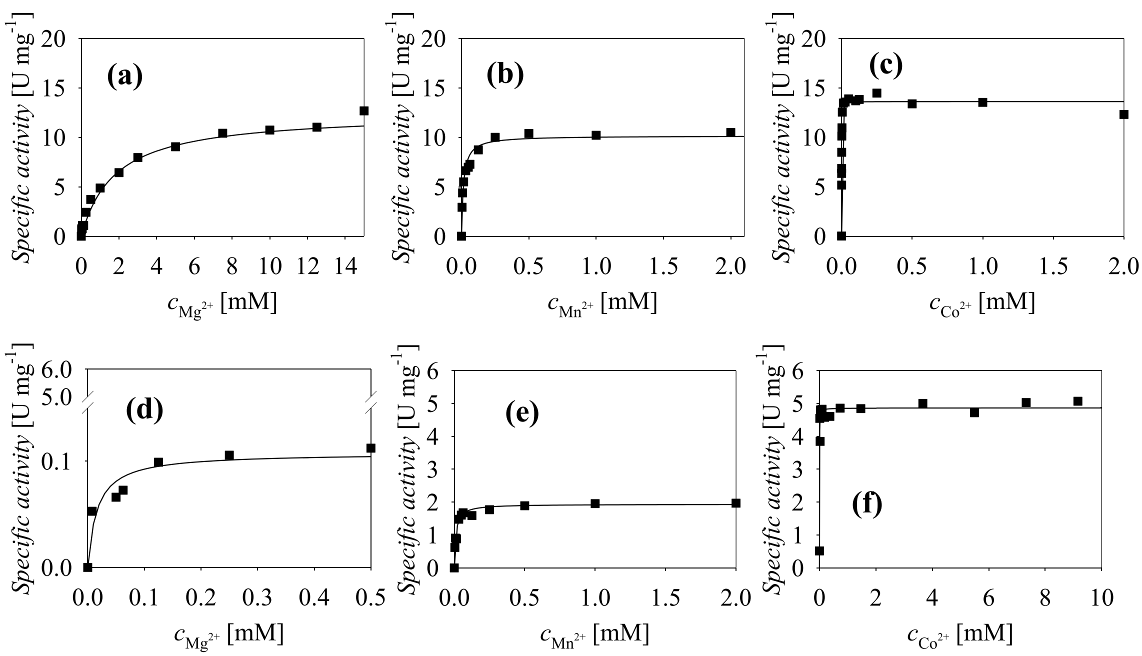

Fig. 5 Dependence of specific enzyme activity on the concentrations of metal cofactors for *Nm*NeuS (**a–c** $c_{ManNAc}=10$ mM, $c_{PEP}=10$ mM, 150 sodium phosphate buffer pH 7.5, 37 °C) and PNH_5 (**d–f** $c_{ManNAc}=20$ mM, $c_{PEP}=20$ mM, 150 sodium acetate buffer pH 5.5, 37 °C, $\gamma_{PNH5}=0.300$ mg mL^{-1}): **a** Mg^{2+} ($\gamma_{NeuS}=0.081$ mg mL^{-1}), **b** Mn^{2+} ($\gamma_{NeuS}=0.330$ mg mL^{-1}), **c** Co^{2+} ($\gamma_{NeuS}=0.33$ mg mL^{-1}), **d** Mg^{2+}, **e** Mn^{2+}, and **f** Co^{2+}

Co^{2+} shown by low apparent K_m values in Table 1. This means that a very low cobalt concentration is necessary to obtain maximum reaction rate, i.e. specific activity.

Kinetics of aldol-like condensation of ManNAc and PEP catalysed by NmNeuS and PNH_5

Having identified Co^{2+} as the optimum cofactor, a thorough investigation of the reaction kinetics was conducted for both enzymes. This means that the influence of ManNAc, co-substrate PEP, and Neu5Ac concentrations on the specific enzyme activity was evaluated. The results presented in Fig. 6. show that for *Nm*NeuS, both ManNAc (Fig. 6a) and PEP (Fig. 6b) behave according to Michaelis–Menten kinetics. It appears that the product, Neu5Ac, does not inhibit the enzyme (Fig. 6c) in the investigated concentration range. Very similar results were obtained with PNH_5 (Fig. 6d) except for the influence of PEP on the enzyme activity (Fig. 6e), where it was found that it mildly inhibits the enzyme as substrate. Kinetic parameters were estimated by using double substrate Michaelis–Menten kinetics from the data presented in Fig. 6. and are presented in Table 1.

Kinetic model of aldol-like addition of ManNAc and PEP

A kinetic model for the aldol-like addition of ManNAc and PEP catalysed by NeuS has not been reported yet to the best of our knowledge. We believe that such research is of great interest considering that modelling holds numerous benefits, such as the ability to simulate different reaction scenarios in silico. Simulations enable choosing the best reactor mode

Table 1 Estimated kinetic parameters of *Nm*NeuS and PNH_5

	*Nm*NeuS		PNH_5		
	V_m [$U \cdot mg^{-1}$]	K_m [mM]	V_m [$U \cdot mg^{-1}$]	K_m [mM]	K_i [mM]
Metal cofactor					
Mn^{2+}	10.157 ± 0.312	0.014 ± 0.002	1.913 ± 0.05	0.010 ± 0.002	-
Mg^{2+}	11.994 ± 0.380	1.384 ± 0.162	0.110 ± 0.009	0.019 ± 0.008	-
Co^{2+}	16.151 ± 0.309	0.0003 ± 0.00005	5.702 ± 0.456	0.0017 ± 0.0008	-
Substrate					
PEP	16.151 ± 0.309	0.991 ± 0.010	5.702 ± 0.456	1.405 ± 0.332	698.997 ± 34.359-
ManNAc		1.353 ± 0.107		0.543 ± 0.139	-

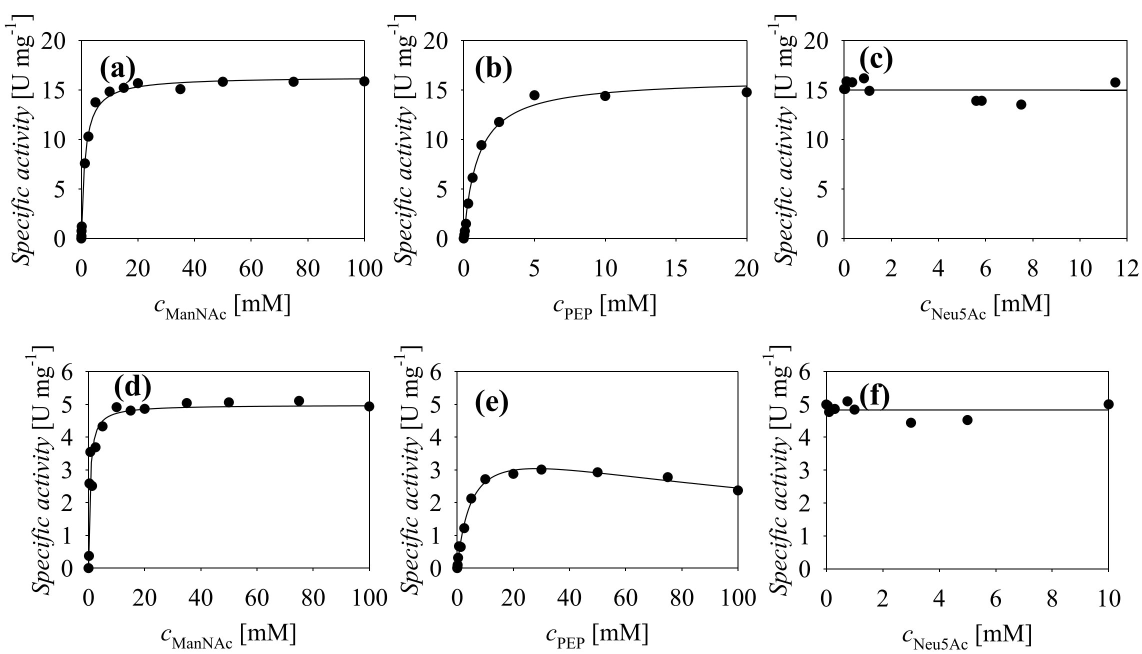

Fig. 6 Dependence of specific enzyme *Nm*NeuS activity (**a–c** $c_{Co^{2+}} = 0.05$ mM, $\gamma_{NeuS} = 0.016$ mg mL^{-1}, 150 mM sodium phosphate buffer pH 7.5) and PNH_5 activity (**d–f** $c_{Co^{2+}} = 0.2$ mM, $\gamma_{PNH5} = 0.015$ mg mL.$^{-1}$, 150 mM sodium acetate buffer pH 5.5) on the concentration of (**a**) ManNAc ($c_{PEP} = 10$ mM), **b** PEP ($c_{ManNAc} = 20$ mM), **c** Neu5Ac ($c_{ManNAc} = 10$ mM, $c_{PEP} = 10$ mM), **d** ManNAc ($c_{PEP} = 10$ mM), **e** PEP ($c_{ManNAc} = 20$ mM), and **f** Neu5Ac ($c_{ManNAc} = 20$ mM, $c_{PEP} = 20$ mM)

and in combination with selection of downstream processing methods make a great base for early stage process cost estimation. This enables comparison of different synthesis methods and process schemes at an early stage of process development. Additionally, it enables the comparison of the estimated product price in the investigated process with the prices on the market. Modelling also enables making assumptions and estimations about the effect of the process on the environment. Most of these benefits were demonstrated before for other reaction systems (Findrik Blažević et al. 2021; Sudar et al. 2021; Česnik Katulić et al. 2021). Based on the presented experimental data (Fig. 6.), a kinetic model was developed (Eqs. (2) and (3)) for the synthesis of Neu5Ac catalysed by *Nm*NeuS and PNH_5, respectively. In these equations, r_1 and r_2 present the reaction rate of Neu5Ac formation. Mass balance equations for ManNAc, PEP, and Neu5Ac in the batch reactor are presented by the Eqs. (5)–(7), respectively. They are vital for the validation of the mathematical model, which was done in the batch system in this case and will be discussed later.

Storage stability of NeuS and PNH_5

We followed the activity and protein concentration of *Nm*NeuS and PNH_5 for 50 days to assess the stability of enzymes during storage. The results presented in Fig. 7. show that *Nm*NeuS retains around 50% of its initial activity after 50 days (Fig. 7a) and forms a kind of equilibrium then, whereas PNH_5 loses all its activity during the same period. As far as the protein concentration is concerned, it remains more or less constant for *Nm*NeuS, whereas for PNH_5, it follows the drop of enzyme activity (Fig. S6, Fig. 7b). It needs to be noted that the data for PNH_5 were measured at pH 7.5 (Fig. S6), as well as 5.5 (Fig. 7b). While the enzyme shows poor stability at pH 7.5, it was shown that the stability is significantly improved at pH 5.5 (Fig. 7b), which is the optimum pH for enzyme activity.

To assess what happens with the protein molecules for 50 days, the DLS technique was performed. Namely, the changes in the enzyme performance during time can be attributed to the changes in its structure. As the enzyme was incubated in the same medium throughout the experiment, the surrounding conditions remained constant, meaning that any changes in the size distribution profile of the enzyme can be attributed solely to structural changes over time, such as enzyme degradation and consequent aggregation during storage. Since both enzymes displayed activity loss to some extent, DLS was performed to determine whether the stability decline could be attributed to the changes in protein structure and, consequently, aggregation. Thus, it makes sense to evaluate what is happening to protein size distributions, namely NSD, VSD, and ISD. The distribution of the particles with different hydrodynamic diameters is presented in Fig. 8. In the initial phase immediately after purification, the particle sizes of *Nm*NeuS were in the range of 10 nm which corresponds to the size of the crystal dimer designated as 58.766 × 76.147 × 77.482 Å (PDB ID: 1XUU (Berman et al. 2003; Gunawan et al. 2005)). Such monomodal and narrow distribution around the size of the crystal protein indicates the existence of the active form of the enzyme in homogeneous mixture. Subsequently, following the initial stage of the purification process, a similar trend was noted with PNH_5 particles, whose dimensions fell within the 10-nm range, aligning with the calculated dimensions, 123.8 × 49.1 × 48.7 Å, derived from an Inertia Axis Aligned Bounding Box (IABB, Draw Protein Dimensions Script (Schrödinger 2015)). Furthermore, it can be concluded from the presented data for this enzyme that the size of the protein molecules is approximately the same as that for *Nm*NeuS (Figs. 8 a and b and 9 c and d, respectively). The similarity in dimensional characteristics between *Nm*NeuS and PNH_5 is evident in the superimposed 3D models illustrated in Fig. 2a. These results

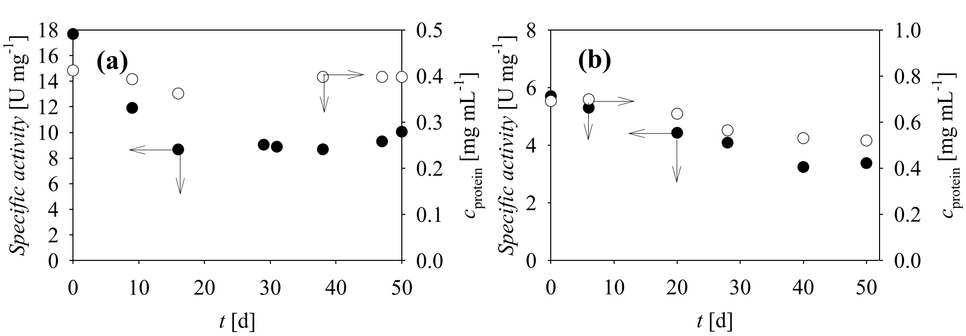

Fig. 7 Storage stability presented as the change of specific activity and protein concentration during 50 days for **a** *Nm*NeuS (150 mM sodium phosphate buffer, pH 7.5, c_{ManNAc} = 10 mM, c_{PEP} = 10 mM, $c_{Co}{}^{2+}$ = 0.05 mM, γ_{NmNeuS} = 0.048 mg mL^{-1}) and **b** PNH_5 (150 mM sodium acetate buffer pH 5.5, c_{ManNAc} = 20 mM, c_{PEP} = 20 mM, $c_{Co}{}^{2+}$ = 0.05 mM, γ_{PNH5} = 0.035 mg mL.$^{-1}$, 37 °C)

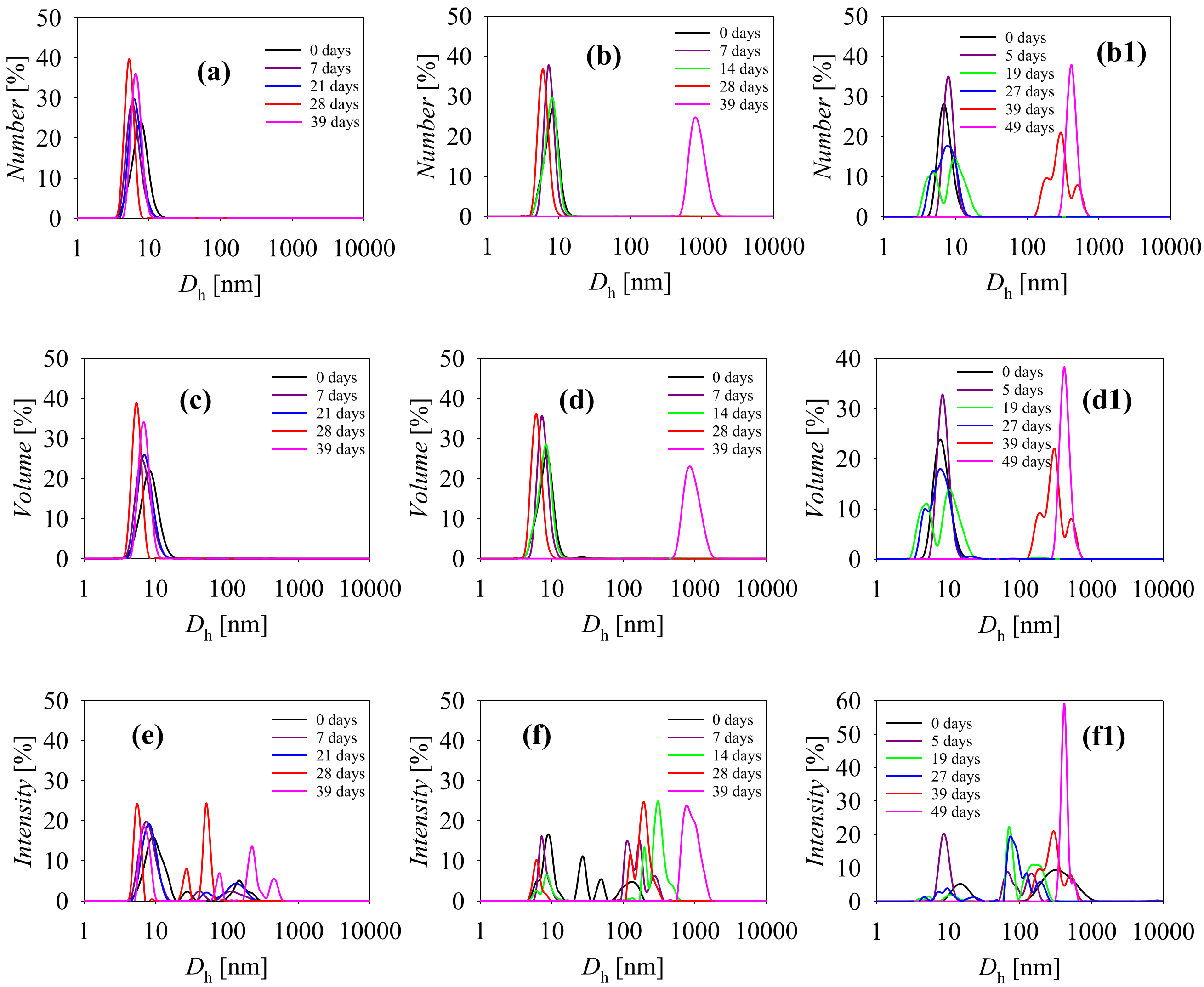

Fig. 8 Size distributions of *Nm*NeuS and PNH_5 in buffer solution during 39–49 days of storage according to the number (**a** *Nm*NeuS, **b–b1** PNH_5), volume (**c** *Nm*NeuS, **d–d1** PNH_5, and intensity (**e** *Nm*NeuS, **f–f1** PNH_5) (γ_{Enzyme} = 1 mg mL.$^{-1}$; 150 mM sodium phosphate buffer pH 7.5 for (**a**), (**b**), (**c**), (**d**), (**e**), and (**f**); 50 mM sodium acetate pH 5.5 for (**b1**), (**d1**), and (**f1**); 4 °C)

indicate a higher protein integrity of *Nm*NeuS than PNH_5 at these conditions. Even after 39 days, *Nm*NeuS does not show visible aggregation when NSD and VSD are studied, while for PNH_5, significant protein aggregation occurred after 39 days in both buffers, which is evident from the shift of the peak at the particle size of 100–1000 nm. These data at pH 7.5 correlate well with the protein concentration and specific activity data presented in Fig. S6. According to NSD, PNH_5 at pH 5.5 appears to be in completely aggregated form after 49 days (Fig. 8b1), although activity measurements show a retention of about 50% of the initial value. This could, for example, be attributed to the change of surface charge of larger aggregates, which at pH 5.5 attract proteins in their active form through electrostatic interactions, potentially complicating their differentiation during DLS measurements. To inspect this further, the sample was centrifuged after 61 days, and the activity, protein concentration and PSD in the supernatant were measured. After separation by centrifugation, the concentration of soluble proteins in the supernatant was 0.297 mg/mL with specific activity 4.80 U/mg. PSD measurements also confirmed the existence of active proteins around 10 nm, which were not detectable by the same method before centrifugation (Fig. S7).

Figure 8e–f1 present the enzyme particle ISD. Since this type of distribution weights particles according to the intensity of the signal, it is convenient for early identification of protein aggregation. These data show that even though the majority of particles correspond to the size of the protein crystal as elaborated in Fig. 8a–d1, both enzymes are prone

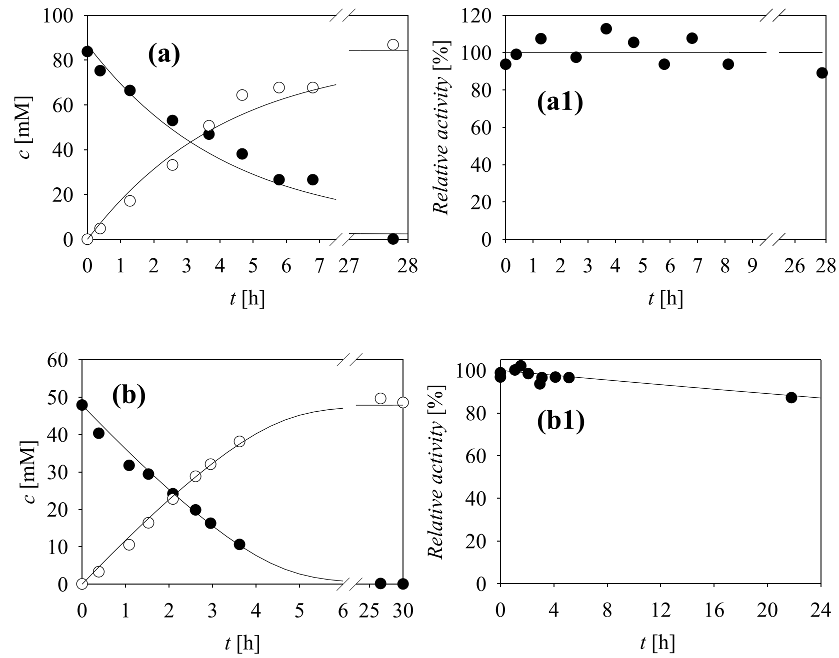

Fig. 9 Synthesis of Neu5Ac catalysed by *Nm*NeuS (150 mM sodium phosphate buffer pH 7.5, 37 °C, $\gamma_{NeuS} = 0.021$ mg mL^{-1}, $c_{Co2+} = 0.05$ mM) and PNH_5 (150 mM sodium acetate buffer pH 5.5, 37 °C, $\gamma_{PNH5} = 0.053$ mg mL^{-1}, $c_{Co2+} = 0.05$ mM) in the batch reactor. **a** $c_{ManNAc} = 83.79$ mM, $c_{PEP} = 100.00$ mM. **a1** Operational stability of *Nm*NeuS during the experiment presented in (**a**). **b** $c_{ManNAc} = 47.90$ mM, $c_{PEP} = 50.00$ mM. **b1** Operational stability of PNH_5 during the experiment presented in (**b**). Legend: **a–b** black circles, ManNAc; white circles, Neu5Ac; black line, simulation. **a1–b1** black circles, relative activity of *Nm*NeuS (**a1**) and PNH_5 (**b1**) during the experiments; black line, model simulation

34

to aggregation to some extent. For *Nm*NeuS, it is less obvious from other data, but Fig. 8e shows that immediately after purification, there are particles in the range of 100 nm (black line). After 39 days, there are particles in the higher size ranges as well. This is more pronounced for PNH_5 (Fig. 8 f and f1) with signals of relatively high intensity for particle sizes up to 1000 nm. This corresponds well to other provided experimental data, i.e. protein concentration and activity. Since after 20 days both enzymes at pH 7.5 retain approximately 50% of the initial activity (Fig. 7a and Fig. S6), and

PNH_5 around 65% at pH 5.5 (Fig. 8b), and the particle size distribution does not detect the formation of the same number of aggregates, it can be concluded that aggregation is not the only and predominant reason for loss of stability. However, the DLS method does not rule out the loss of activity due to other conformational changes such as dimer dissociation into monomers. The size difference between these units is not sufficient for the method resolution, as the factor of 3 is a prerequisite for the successful detection of definite change in size by this experimental method. In the case of PNH_5 at pH 7.5, the drop in protein concentration after 50 days (Fig. S6) can be attributed to the formation of water-insoluble protein aggregates, as clearly confirmed by DLS.

Mathematical model simulations and the stability of enzyme during the reaction

The mathematical model of Neu5Ac synthesis was validated in a series of batch reactor experiments (Eqs. (2) and (4)–(7)). The synthesis of Neu5Ac catalysed by NeuS is a double substrate reaction that starts from ManNAc and PEP. The reaction therefore requires PEP in stoichiometric amounts as co-substrate and an addition of metal cofactor. Co^{2+} was found to be the best choice and was therefore used in further experiments. The first series of experiments was performed with *Nm*NeuS and is presented in Fig. 9 a and a1 and Fig. S8. During the experiments, enzyme activity was evaluated, and the results are also presented in Fig. 9a1 and Fig. S8 a1 and b1. The operational stability is an enzyme property crucial for its application. It was evaluated by following enzyme activity in a series of batch reactor experiments.

Figure 9a and Fig. S8a–c show the change of concentrations of ManNAc and Neu5Ac during the experiment for the reaction catalysed by *Nm*NeuS, whereas Fig. 9a1and Fig. S8a1–b1 show the change in the enzyme activity during the experiments. In all the cases, it can be observed that the mathematical model describes the data well and that the enzyme activity is practically constant implying that *Nm*NeuS has good operational stability. Batch reactor experiments at different reaction conditions were conducted with PNH_5 as well and are presented in Fig. 9b and Fig. S9. The mathematical model (Eqs. (3) and (4)–(7)) also described the data well. Thus, it can be verified for both enzymes that product inhibition is not present as assumed from the limited concentration range measurements. The experiment presented in Fig. S9b1 shows that the enzyme operational stability is good at the reaction conditions. Figure 9b1 shows that a slow enzyme activity drop can be observed in case of the experiment conducted at 50 mM of substrate. The operational stability decay rate constant of the first order was estimated to be $k_d = 9.6 \cdot 10^{-5} \pm 9.2 \cdot 10^{-6}$ min^{-1}. This value corresponds to 120.34 h enzyme half-life time. In the case of the experiment presented in Fig. S9c, the operational stability decay rate constant was estimated directly from the concentration vs. time data. It was found to be 0.0015 ± 0.0001 min^{-1}, corresponding to the enzyme half-life time of 7.7 h. Thus, it appears that for this enzyme, an increase of substrate concentration also means a decrease in enzyme operational stability. Statistical output of the mathematical model, along with the explanation of its meaning is presented in Table S3.

Discussion

On the effect of pH on NeuS activity

A wide range of pH values have showed compatibility with NeuS activity from different organisms (Table S1), but the pH optimums reported were always in the same range between 7.0 and 8.3. For comparison, at the respective pH values, PNH_5 displays only around 20% of its maximum activity observed at 5.5. At pH 5.0, PNH_5 activity drops by 50%, whereas a complete activity loss is observed at pH 4.0. However, while pH 7.0 is an optimum for *Sa*NeuS activity, *As*NeuS was inactive at the same pH (Suryanti et al. 2003; Gurung et al. 2013). Furthermore, *As*NeuB becomes active from its inactive form when pH is increased from 7.0 to 7.5, in accordance with *Nm*NeuS activity (Blacklow and Warren 1962; Hao et al. 2005; Gurung et al. 2013). As the mechanistic studies have shown that the metal ions are vital for bacterial NeuS catalysis, a change in the protonation states of the metal ion coordinating the active site histidines (His215 and His236) could explain the increase in the activity (Gurung et al. 2013; Berg et al. 2015).

On the influence of cofactors on the activity of *Nm*NeuS and PNH_5 and enzyme kinetics

As stated before, in the relevant literature, several divalent metal cofactors were tested with NeuS homologues, i.e. magnesium, manganese, cobalt, calcium, and others (Blacklow and Warren 1962; Vann et al. 1997; Linton et al. 2000; Suryanti et al. 2003; Sundaram et al. 2004; Gunawan et al. 2005; Hao et al. 2005; Liu et al. 2009; Gurung et al. 2013; García García et al. 2015; Berg et al. 2015). For example, Hao et al. (2005) reported that the activity of *Nm*NeuS was around 2.7-fold higher in the presence of cobalt than magnesium ions, while it was around 1.15-fold better in the presence of manganese than magnesium ions. Komaki et al. (1997) reported that NeuS from *E. coli* K1-M12 does not need a metal cofactor for enzyme activity. In most of these reports, some research on the cofactor effect was done. However, systematic studies on the effect of cofactor concentration on enzyme activity had not been reported so far. Such experiments are important to find the optimum conditions for enzyme activity in the reactor for producing sialic acid analogues. Additionally, none of the authors so far stated that they considered the metal cofactors already present in the enzyme samples after the purification. Therefore, we believe that Komaki et al. (1997) may have falsely reported that their enzyme needs no cofactor for activity. As a major difference to research done so far, all our measurements were performed with purified enzyme, from which the metal cofactors were previously removed by the EDTA treatment (Mónico et al. 2017). An ICP-MS analysis was performed to prove the absence of metals, which could affect enzyme activity (Table S2). We could detect only Mn^{2+} and Ni^{2+} in the purified enzyme samples, corresponding to the native cofactor and the affinity purification reagent. Enzyme preparations containing no metal after EDTA treatment did not exhibit activity in the synthesis of Neu5Ac. During enzyme production and purification, various metal ions present in solution may bind to the enzyme and affect the measured enzyme activity. If the bound metal had not been removed before, it would be difficult to judge the effect on enzyme activity of systematically adding different metal cofactors and their concentration, when the enzymes independently showed dubious activity even in the absence of added metal ions.

While some kinetic parameters can be found in the literature for *Nm*NeuS, as well as for other enzymes (Table S1), the data is scarce and not measured in a systematic fashion. In addition, different methods and assays were applied. While Hao et al. (2005) reported k_{cat} value of 49.5 min^{-1} for this enzyme, in our case, it is estimated to be significantly higher at 619.41 ± 11.81 min^{-1}. It needs to be noted here that we used broader concentration ranges of substrate and co-substrate in our measurements and non-linear regression analysis to estimate the values of the kinetic parameters. Additionally, the Michaelis constant for ManNAc was estimated to be almost tenfold lower in our case, and the value of k_{cat}/K_m was 7644.4 s^{-1} M^{-1}. These differences come from the experimental and data handling methodology. Namely, Hao et al. (2005) applied a colorimetric TBA assay and used 1 mM Mg^{2+} as a cofactor, even though they also concluded that Co^{2+} yields a three-fold better enzyme activity. Additionally, they used different buffers and a rather narrow concentration range of ManNAc only up to 3 mM, which is significantly lower than the Michaelis constant they estimated for *Nm*NeuS.

As far as PNH_5 is concerned, the estimated Michaelis constants for PEP and ManNAc (Table 1) are quite low and comparable to *Nm*NeuS meaning that ManNAc is an excellent substrate for this enzyme, and a good selection if, for some chemical reason, acidic pH is required. For example, this could be interesting for downstream processing purposes without the need for media exchange, possibly leading to a more profitable process, because Furuhata (2004) reported that sialic acids crystallize from water–acetic acid mixtures (Furuhata 2004).

The analysis of the molecular structure of PNH_5 revealed that the molecular weight of the enzyme to be 38.4 kDa, k_{cat} was calculated to be 219.01 ± 18.05 min^{-1} and k_{cat}/K_m was estimated to be 6755 s^{-1} M^{-1}.

On the storage stability of NeuS and PNH_5

Enzyme stability is an important feature of every industrial biocatalyst. It is therefore important to evaluate it and improve it if needed. As far as NeuS homologues are concerned, no systematic study of enzyme stability was reported so far to the best of our knowledge. Hwang et al. (2002) identified site-specific cleavage prone to proteolysis identified at Lys280 residue for *Ec*NeuS and concluded that the purified enzyme, identified as tetramer (160 kDa), was not susceptible to cleavage. They described the degradation of monomer (size 40 kDa) to two different fractions, e.g. 33 and 7 kDa, and suspected that in that manner, the tetramer turns to trimer and loses the activity. Suryanti et al. (2003) reported that *Sa*NeuS was prone to proteolysis during purification. Sundaram et al. (2004) reported that pure *Cj*NeuS was not very stable, and for that reason, they conducted experiments with partially purified enzyme. Hao et al. (2005) reported that the recombinant *Nm*NeuS is stable when stored at −20 °C. The cold-adapted *Mv*NeuS (Berg et al. 2015) was found to be stable for 3–4 weeks at 4 °C, but readily aggregated at room temperature. They performed a calorimetric study, which showed that the enzyme unfolds with a two-step transition, i.e. two peaks indicated that the dimer first separates into monomers (1st peak) and that monomers deactivate at higher temperatures (2nd peak).

From the presented literature overview, it is evident that the data is insufficient to understand what is going on with these enzymes in the solution, and that is why we combined enzyme activity and protein concentration measurements with DLS technique to elucidate the situation.

On the application of the mathematical model and the operational stability of enzymes

When discussing the optimal reaction conditions and design, one must have a deep insight into the kinetic behaviour of an enzyme. In case of *Nm*NeuS, we can see that the reaction kinetics is very simple double substrate Michaelis–Menten kinetics. In these cases, the selection of a reactor mode is less difficult. If an enzyme is stable, such as in the *Nm*NeuS case, any reactor will be applicable and good. However, if we aim towards high volumetric productivity, a continuous reactor mode would be the best option ensuring constant product quality (Fig. S10 for *Nm*NeuS). In order to ensure good enzyme reusability, an ultrafiltration membrane reactor can be applied (Sudar et al. 2013; Valinger et al. 2014). However, the limitation of Neu5Ac solubility means that the highest substrate concentration should be in the range of 160 mM. Alternative continuous systems would require enzyme immobilization. In case of PNH_5, PEP inhibition is mild, and does not really affect the outcome. However, since enzyme stability seems to be a potential issue, enzyme immobilization could be considered for further application. Instead, discontinuous reactor modes can also be applied. The results collected so far represent an excellent platform for the application of NeuS in the synthesis of unnatural sugars, while it is expected that the findings presented in this work can be generalized on other potential reactions catalysed by these enzymes. Our current research is directed toward that area.

Supplementary Information The online version contains supplementary material available at https://doi.org/10.1007/s00253-024-13277-1.

Author contribution MMÇ, NM, and TA conducted experiments. MMÇ, NM, and ZFB designed the research. NM, ZFB, and SC supervised the research. ZFB, SC, and WDF acquired resources. ZFB, SC, and WDF acquired funding. All authors wrote, read, and approved the manuscript.

Funding This project has received funding from the European Union's Horizon 2020 research and innovation programme under the Marie Sklodowska-Curie grant agreement no. 956631 (CC-TOP).

Data availability The data that supports the findings of this study are available in the supplementary material of this article.

Declarations

Ethical approval This article does not contain any studies with human participants or animals performed by any of the authors.

Conflict of interest The authors declare no competing interests.

References

Baardsnes J, Davies PL (2001) Sialic acid synthase: the origin of fish type III antifreeze protein? Trends Biochem Sci 26:468–469. https://doi.org/10.1016/S0968-0004(01)01879-5

Bateman A, Martin MJ, Orchard S, Magrane M, Agivetova R, Ahmad S, Alpi E, Bowler-Barnett EH, Britto R, Bursteinas B, Bye-A-Jee H, Coetzee R, Cukura A, da Silva A, Denny P, Dogan T, Ebenezer TG, Fan J, Castro LG, Garmiri P, Georghiou G, Gonzales L, Hatton-Ellis E, Hussein A, Ignatchenko A, Insana G, Ishtiaq R, Jokinen P, Joshi V, Jyothi D, Lock A, Lopez R, Luciani A, Luo J, Lussi Y, MacDougall A, Madeira F, Mahmoudy M, Menchi M, Mishra A, Moulang K, Nightingale A, Oliveira CS, Pundir S, Qi G, Raj S, Rice D, Lopez MR, Saidi R, Sampson J, Sawford T, Speretta E, Turner E, Tyagi N, Vasudev P, Volynkin V, Warner K, Watkins X, Zaru R, Zellner H, Bridge A, Poux S, Redaschi N, Aimo L, Argoud-Puy G, Auchincloss A, Axelsen K, Bansal P, Baratin D, Blatter MC, Bolleman J, Boutet E, Breuza L, Casals-Casas C, de Castro E, Echioukh KC, Coudert E, Cuche B, Doche M, Dornevil D, Estreicher A, Famiglietti ML, Feuermann M, Gasteiger E, Gehant S, Gerritsen V, Gos A, Gruaz-Gumowski N, Hinz U, Hulo C, Hyka-Nouspikel N, Jungo F, Keller G, Kerhornou A, Lara V, Le Mercier P, Lieberherr D, Lombardot T, Martin X, Masson P, Morgat A, Neto TB, Paesano S, Pedruzzi I, Pilbout S, Pourcel L, Pozzato M, Pruess M, Rivoire C, Sigrist C, Sonesson K, Stutz A, Sundaram S, Tognolli M, Verbregue L, Wu CH, Arighi CN, Arminski L, Chen C, Chen Y, Garavelli JS, Huang H, Laiho K, McGarvey P, Natale DA, Ross K, Vinayaka CR, Wang Q, Wang Y, Yeh LS, Zhang J, Ruch P, Teodoro D (2021) UniProt: the universal protein knowledgebase in 2021. Nucleic Acids Res 49:D480–D489. https://doi.org/10.1093/nar/gkaa1100

Berg TO, Gurung MK, Altermark B, Smalås AO, Ræder ILU (2015) Characterization of the N-acetylneuraminic acid synthase (NeuB) from the psychrophilic fish pathogen *Moritella viscosa*. Carbohyd Res 402:133–145

Berman H, Henrick K, Nakamura H (2003) Announcing the worldwide Protein Data Bank. Nat Struct Biol 10:980

Blacklow RS, Warren L (1962) Biosynthesis of sialic acids by *Neisseria meningitidis*. J Biol Chem 237:3520–3526. https://doi.org/10.1016/s0021-9258(19)70850-3

Bradford M (1976) A rapid and sensitive method for the quantitation of microgram quantities of protein utilizing the principle of protein-dye binding. Anal Biochem 72:248–254. https://doi.org/10.1006/abio.1976.9999

Česnik Katulić M, Sudar M, Hernández K, Qi Y, Charnock SJ, Vasić-Rački Đ, Clapés P, Findrik Blažević Z (2021) Cascade synthesis of L-homoserine catalyzed by lyophilized whole cells containing transaminase and aldolase activities: the mathematical modeling approach. Ind Eng Chem Res 60:13846–13858. https://doi.org/10.1021/acs.iecr.1c02343

Česnik M, Sudar M, Roldan R, Hernandez K, Parella T, Clapés P, Charnock S, Vasić-Rački Đ, Findrik Blažević Z (2019) Model-based optimization of the enzymatic aldol addition of propanal to formaldehyde: a first step towards enzymatic synthesis of 3-hydroxybutyric acid. Chem Eng Res Des 150:140–152. https://doi.org/10.1016/j.cherd.2019.06.025

Colley KJ, Kitajima K, Sato C (2014) Polysialic acid: biosynthesis, novel functions and applications. Crit Rev Biochem Mol Biol 49:498–532. https://doi.org/10.3109/10409238.2014.976606

Cunningham BA, Hoffman S, Rutishauser U, Hemperly JJ, Edelman GM (1983) Molecular topography of the neural cell adhesion molecule N-CAM: surface orientation and location of sialic acid-rich and binding regions. PNAS 80:3116–3120. https://doi.org/10.1073/pnas.80.10.3116

Eastman P, Swails J, Chodera JD, McGibbon RT, Zhao Y, Beauchamp KA, Wang L-P, Simmonett AC, Harrigan MP, Stern CD, Wiewiora RP, Brooks BR, Pande VS (2017) OpenMM 7: Rapid development of high performance algorithms for molecular dynamics. PLOS Comput Biol 13. https://doi.org/10.1371/journal.pcbi.1005659

Fessner WD, He N, Yi D, Unruh P, Knorst M (2014) Enzymatic Generation of Sialoconjugate Diversity. In: Riva S, Fessner W-D (eds) Cascade biocatalysis: integrating stereoselective and environmentally friendly reactions. Wiley-VCH Verlag GmbH & Co, KGaA, pp 361–392

Findrik Blažević Z, Milčić N, Sudar M, Majerić Elenkov M (2021) Halohydrin dehalogenases and their potential in industrial application – a viewpoint of enzyme reaction engineering. Adv Synth Catal 363:388–410. https://doi.org/10.1002/adsc.202000984

Fukuda M (1996) Possible roles of tumor-associated carbohydrate antigens. Cancer Res 56:2237–2244

Furuhata K (2004) Chemistry of N-acetylneuraminic acid (Neu5Ac). Trends Glycosci Glyc 16:143–169

García García MI, Lau K, Von Itzstein M, García Carmona F, Sánchez Ferrer Á (2015) Molecular characterization of a new N-acetylneuraminate synthase (NeuB1) from *Idiomarina loihiensis*. Glycobiol 25:115–123. https://doi.org/10.1093/glycob/cwu096

Garrabou X, Castillo JA, Guérard-Hélaine C, Parella T, Joglar J, Lemaire M, Clapés P (2009) Asymmetric self- and cross-aldol reactions of glycolaldehyde catalyzed by D-fructose-6-phosphate aldolase. Angew Chem Int Ed 48:5521–5525. https://doi.org/10.1002/anie.200902065

Gasteiger E, Hoogland C, Gattiker A, Duvaud S, Wilkins MR, Appel RD, Bairoch A (2005) Protein identification and analysis tools on the ExPASy server. In: Walker JM (ed) The Proteomics Protocols Handbook. Humana Press, Totowa, NJ, pp 571–607

Gorelik E, Galili U, Raz A (2001) On the role of cell surface carbohydrates and their binding proteins (lectins) in tumor metastasis. Cancer Metastasis Rev 20:245–277

Gunawan J, Simard D, Gilbert M, Lovering AL, Wakarchuk WW, Tanner ME, Strynadka NCJ (2005) Structural and mechanistic analysis of sialic acid synthase NeuB from *Neisseria meningitidis* in complex with Mn^{2+}, phosphoenolpyruvate, and N-acetylmannosaminitol. J Biol Chem 280:3555–3563. https://doi.org/10.1074/jbc.M411942200

Gurung MK, Ræder IL, Altermark B, Smalås AO (2013) Characterization of the sialic acid synthase from *Aliivibrio salmonicida* suggests a novel pathway for bacterial synthesis of 7-O-acetylated sialic acids. Glycobiol 23:806–819. https://doi.org/10.1093/glycob/cwt018

Hao J, Balagurumoorthy P, Sarilla S, Sundaramoorthy M (2005) Cloning, expression, and characterization of sialic acid synthases. Biochem Biophys Res Comm 338:1507–1514. https://doi.org/10.1016/j.bbrc.2005.10.113

He N, Yi D, Fessner W (2011) Flexibility of substrate binding of cytosine-5′-monophosphate- *n* -acetylneuraminate synthetase (CMP-sialate synthetase) from *Neisseria meningitidis*: an enabling catalyst for the synthesis of neo-sialoconjugates. Adv Synth Catal 353:2384–2398. https://doi.org/10.1002/adsc.201100412

Heida R, Bhide YC, Gasbarri M, Kocabiyik Ö, Stellacci F, Huckriede ALW, Hinrichs WLJ, Frijlink HW (2021) Advances in the development of entry inhibitors for sialic-acid-targeting viruses. Drug Discov Today 26:122–137. https://doi.org/10.1016/j.drudis.2020.10.009

Hwang TS, Hung CH, Teo CF, Chen GT, Chang LS, Chen SF, Chen YJ, Lin CH (2002) Structural characterization of *Escherichia coli* sialic acid synthase. Biochem Biophys Res Commun 295:167–173. https://doi.org/10.1016/S0006-291X(02)00620-4

Joseph DDA, Jiao W, Kessans SA, Parker EJ (2014) Substrate-mediated control of the conformation of an ancillary domain delivers a competent catalytic site for N-acetylneuraminic acid synthase. Proteins: Structure. Function and Bioinformatics 82:2054–2066. https://doi.org/10.1002/prot.24558

Joseph DDA, Jiao W, Parker EJ (2013) Arg314 Is essential for catalysis by N-acetyl neuraminic acid synthase from *Neisseria meningitidis*. Biochem 52:2609–2619. https://doi.org/10.1021/bi400062c

Keil JM, Rafn GR, Turan IM, Aljohani MA, Sahebjam-Atabaki R, Sun X-L (2022) Sialidase inhibitors with different mechanisms. J Med Chem 65:13574–13593. https://doi.org/10.1021/acs.jmedchem.2c01258

Kiefel MJ, Von Itzstein M (2002) Recent advances in the synthesis of sialic acid derivatives and sialylmimetics as biological probes. Chem Rev 102:471–490. https://doi.org/10.1021/cr000414a

Knorst M (1999) Neue Enzyme zur Synthese von sialinsäurehaltigen Oligosacchariden. Aachen Techn Hochsch Diss

Koketsu M, Nitoda T, Sugino H, Juneja LR, Kim M, Yamamoto T, Abe N, Kajimoto T, Wong C-H (1997) Synthesis of a novel sialic acid derivative (sialylphospholipid) as an antirotaviral agent. J Med Chem 40:3332–3335. https://doi.org/10.1021/jm9701280

Komaki E, Otha Y, Tsukada Y (1997) Purification and characterization of n-acetylneuraminate synthase from *Escherichia coli* kl-m12. Biosci, Biotechnol Biochem 61:2046–2050. https://doi.org/10.1271/bbb.61.2046

Laemmli UK (1970) Cleavage of structural proteins during the assembly of the head of bacteriophage T4. Nature 227:680–685. https://doi.org/10.1038/227680a0

Linton D, Karlyshev AV, Hitchen PG, Morris HR, Dell A, Gregson NA, Wren BW (2000) Multiple N-acetyl neuraminic acid synthetase (neuB) genes in *Campylobacter jejuni*: Identification and characterization of the gene involved in sialylation of lipo-oligosaccharide. Mol Microbiol 35:1120–1134. https://doi.org/10.1046/j.1365-2958.2000.01780.x

Liu F, Lee HJ, Strynadka NCJ, Tanner ME (2009) Inhibition of *Neisseria meningitidis* sialic acid synthase by a tetrahedral intermediate analogue. Biochem 48:9194–9201. https://doi.org/10.1021/bi9012758

Mahmoudian M, Noble D, Drake CS, Middleton RF, Montgomery DS, Piercey JE, Ramlakhan D, Todd M, Dawson MJ (1997) An efficient process for production of N-acetylneuraminic acid using N-acetylneuraminic acid aldolase. Enzyme Microb Technol 20:393–400. https://doi.org/10.1016/S0141-0229(96)00180-9

Marshall JR, Yao P, Montgomery SL, Finnigan JD, Thorpe TW, Palmer RB, Mangas-Sanchez J, Duncan RAM, Heath RS, Graham KM, Cook DJ, Charnock SJ, Turner NJ (2021) Screening and characterization of a diverse panel of metagenomic imine reductases for biocatalytic reductive amination. Nat Chem 13:140–148. https://doi.org/10.1038/s41557-020-00606-w

Mertsch A, He N, Yi D, Kickstein M, Fessner WD (2020) An α2,3-Sialyltransferase from *Photobacterium phosphoreum* with Broad Substrate Scope: Controlling Hydrolytic Activity by Directed Evolution. Chem Eur J 26:11614–11624

Mertsch A, Poschenrieder S, Fessner WD (2020) Semi-synthetic sialic acid probes for challenging the substrate promiscuity of enzymes in the sialoconjugation pathway. Adv Synth Catal 362:5485–5495. https://doi.org/10.1002/adsc.202000859

Milčić N, Stepanić V, Crnolatac I, Findrik Blažević Z, Brkljača Z, Majerić Elenkov M (2022) Inhibitory effect of DMSO on halohydrin dehalogenase: experimental and computational insights into the influence of an organic co-solvent on the structural and catalytic properties of a biocatalyst. Chem Eur J 28:e202201923. https://doi.org/10.1002/chem.202201923

Mirdita M, Schütze K, Moriwaki Y, Heo L, Ovchinnikov S, Steinegger M (2022) ColabFold: making protein folding accessible to all. Nat Methods 19:679–682. https://doi.org/10.1038/s41592-022-01488-1

Mirdita M, Steinegger M, Söding J (2019) MMseqs2 desktop and local web server app for fast, interactive sequence searches.

Bioinformatics 35:2856–2858. https://doi.org/10.1093/bioinformatics/bty1057

Mirdita M, von den Driesch L, Galiez C, Martin MJ, Söding J, Steinegger M (2017) Uniclust databases of clustered and deeply annotated protein sequences and alignments. Nucleic Acids Res 45:D170–D176. https://doi.org/10.1093/nar/gkw1081

Mitchell AL, Almeida A, Beracochea M, Boland M, Burgin J, Cochrane G, Crusoe MR, Kale V, Potter SC, Richardson LJ, Sakharova E, Scheremetjew M, Korobeynikov A, Shlemov A, Kunyavskaya O, Lapidus A, Finn RD (2019) MGnify: the microbiome analysis resource in 2020. Nucleic Acids Res. https://doi.org/10.1093/nar/gkz1035

Mónico A, Martínez-Senra E, Cañada FJ, Zorrilla S, Pérez-Sala D (2017) Drawbacks of dialysis procedures for removal of EDTA. PLoS ONE 12:e0169843. https://doi.org/10.1371/journal.pone.0169843

Robert X, Gouet P (2014) Deciphering key features in protein structures with the new ENDscript server. Nucleic Acids Res 42:W320–W324. https://doi.org/10.1093/nar/gku316

Schnaar RL, Gerardy-Schahn R, Hildebrandt H (2014) Sialic acids in the brain: gangliosides and polysialic acid in nervous system development, stability, disease, and regeneration. Physiol Rev 94:461–518. https://doi.org/10.1152/physrev.00033.2013

Schnellbächer M (2017) Kinetische und präparative Studien mit neuen Sialinsäuresynthasen aus *Neisseria meningitidis* und *Campylobacter jejuni*. Ph.D. Thesis, Technische Universität Darmstadt

Schrödinger LLC (2015) The PyMOL Molecular Graphics System. Version 1:8

Sievers F, Wilm A, Dineen D, Gibson TJ, Karplus K, Li W, Lopez R, McWilliam H, Remmert M, Söding J, Thompson JD, Higgins DG (2011) Fast, scalable generation of high-quality protein multiple sequence alignments using Clustal Omega. Mol Syst Biol 7:539–539. https://doi.org/10.1038/msb.2011.75

Steinegger M, Meier M, Mirdita M, Vöhringer H, Haunsberger SJ, Söding J (2019) HH-suite3 for fast remote homology detection and deep protein annotation. BMC Bioinform 20:473. https://doi.org/10.1186/s12859-019-3019-7

Stetefeld J, McKenna SA, Patel TR (2016) Dynamic light scattering: a practical guide and applications in biomedical sciences. Biophys Rev 8:409–427. https://doi.org/10.1007/s12551-016-0218-6

Sudar M, Česnik M, Clapés P, Pohl M, Vasić-Rački Đ, Findrik Blažević Z (2021) A cascade reaction for the synthesis of D-fagomine precursor revisited: kinetic insight and understanding of the system. New Biotechnol 63:19–28. https://doi.org/10.1016/j.nbt.2021.02.004

Sudar M, Findrik Z, Vasić-Rački Đ, Clapés P, Lozano C (2013) Mathematical model for aldol addition catalyzed by two D-fructose-6-phosphate aldolases variants overexpressed in *E. coli*. J Biotechnol 167:191–200. https://doi.org/10.1016/j.jbiotec.2013.07.008

Sundaram AK, Pitts L, Muhammad K, Wu J, Betenbaugh M, Woodard RW, Vann WF (2004) Characterization of N-acetylneuraminic acid synthase isoenzyme 1 from *Campylobacter jejuni*. Biochem J 383:83–89. https://doi.org/10.1042/BJ20040218

Suryanti V, Nelson A, Berry A (2003) Cloning, over-expression, purification, and characterisation of N-acetylneuraminate synthase from *Streptococcus agalactiae*. Prot Expr Purif 27:346–356. https://doi.org/10.1016/S1046-5928(02)00633-2

Traving C, Schauer R (1998) Structure, function and metabolism of sialic acids. Cell Mol Life Sci 54:1330–1349. https://doi.org/10.1007/s000180050258

Valinger D, Vrsalović Presečki A, Kurtanjek Ž, Pohl M, Findrik Blažević Z, Vasić-Rački Đ (2014) Continuous enzymatic carboligation of benzaldehyde and acetaldehyde in an enzyme ultrafiltration membrane reactor and laminar flow microreactors. J Mol Catal B Enzym 102:132–137. https://doi.org/10.1016/j.molcatb.2014.02.003

van Kempen M, Kim SS, Tumescheit C, Mirdita M, Lee J, Gilchrist CLM, Söding J, Steinegger M (2023) Fast and accurate protein structure search with Foldseek. Nat Biotechnol. https://doi.org/10.1038/s41587-023-01773-0

Vann WF, Tavarez JJ, Crowley J, Vimr E, Silver RP (1997) Purification and characterization of the *Escherichia coli* K1 neuB gene product N-acetylneuraminic acid synthetase. Glycobiology 7:697–701. https://doi.org/10.1093/glycob/7.5.697

Varki A (1993) Biological roles of oligosaccharides: all of the theories are correct. Glycobiology 3:97–130. https://doi.org/10.1093/glycob/3.2.97

Varki A (1997) Sialic acids as ligands in recognition phenomena. FASEB J 11:248–255. https://doi.org/10.1096/fasebj.11.4.9068613

von Itzstein M, Thomson RJ (1997) Sialic acids and sialic acid-recognising proteins: drug discovery targets and potential glycopharmaceuticals. Curr Med Chem 4:185–210. https://doi.org/10.2174/0929867304666220313111728

Warwel M, Fessner W-D (2000) Indium-mediated chain-extension: an improved protocol for the concise, diastereospecific synthesis of KDN and other sialic acids. Synlett 2000:865–867. https://doi.org/10.1055/s-2000-6693

Yi D, He N, Kickstein M, Metzner J, Weiß M, Berry A, Fessner W (2013) Engineering of a cytidine 5′-monophosphate-sialic acid synthetase for improved tolerance to functional sialic acids. Adv Synth Catal 355:3597–3612. https://doi.org/10.1002/adsc.201300568

Zhang Y, Tao F, Du M, Ma C, Qiu J, Gu L, He X, Xu P (2010) An efficient method for N-acetyl-D-neuraminic acid production using coupled bacterial cells with a safe temperature-induced system. Appl Microbiol Biotechnol 86:481–489. https://doi.org/10.1007/s00253-009-2302-3